Dyakonov surface magnons and magnon polaritons

Shaopeng Hao, Shufang Fu, Sheng Zhou, and Xuan-Zhang Wang[*]

Key Laboratory for Photonic and Electronic Bandgap Materials, Chinese Ministry of Education,
and School of Physics and Electronic Engineering, Harbin Normal University, Harbin 150025, China

We predicted one Dyakonov surface magnon (DSM) and two Dyakonov magnon polaritons (DSMPs) localized at the antiferromagnet (AF)-air interface. Their concise dispersion equations and necessary conditions of existence were obtained. The DSM is the magnetostatic limit of the first DSMP, which are situated inside the AF reststrahlen frequency band. The second DSMP has no magnetostatic limit and lies outside the frequency band. The specifical frequency ranges occupied by the DSM and DSMPs were analytically found. The DSMPs are hybrid-polarization surface polaritons and the DSM is a hybrid-polarization surface magnetostatic mode. The first DSMP possesses large attenuation constants so that it is highly localized at the surface. Compared with it, the second DSMP exhibits relatively small attenuation constants. According to the features of polarization obtained for either DSMP, we used the TE and TM radiations incident on the AF surface to calculate attenuated total reflection (ATR) spectra, respectively. These ATR spectra not only further prove the existence of the DSMPs but also demonstrate their observability in experiment. However, the DSM should be detected by means of a light-scattering technique.

I. INTRODUCTION

It has been well known that there is a hybrid-polarization surface wave localized at the interface between isotropic and anisotropic transparent dielectrics, i.e., the Dyakonov surface wave (DSW) [1–3], where the permittivity principal values of the anisotropic dielectric are different positive constants. Dyakonov originally predicted the DSW and obtained the dispersion relation between the propagation angle and wave vector in the isotropic-frequency plane. Due to the harsh condition for the existence of DSW, it can exist only in a tiny angle domain in the propagation plane so that it was demonstrated in experiment 20 y later [2]. The DSW theory has been extended to various interface structures, for example the free-space/photonic crystal [4], metamaterials [5–8], or hyperbolic materials [9–12]. The large anisotropy of effective dielectric permittivity in the artificial structures or hyperbolic materials leads to a large angle domain of DSW propagation so that the DSW is easier to be observed. Therefore, a new window was opened for potential applications of this kind of surface electromagnetic waves.

Hyperbolic metamaterials and naturally hyperbolic crystals have a unique permittivity with opposite-sign principal values and can support various DSWs [5,6,9]. DSWs supported by metamaterials including noble-metal constituent are surface plasmon polaritons [5,11], but those supported by hyperbolic crystals [9,10] or metamaterials including polar-crystal constituent are surface phonon polaritons [6]. From the relevant works mentioned above, one can recognize that these surface waves or polaritons originate from the dielectric anisotropy of materials, i.e., the anisotropy of permittivity.

One naturally wonders if the anisotropy of magnetic permeability in magnetically ordering materials can support Dyakonov surface magnon polaritons (DSMPs). If it is true, what are features of DSMPs? We will answer these questions in this paper. Antiferromagnets (AFs) form a big family, including transition-metal fluorides and oxides, as well as metal antiferromagnets. We will focus on a simple insulative AF, such as transition-metal fluoride FeF_2 or MnF_2, to seek DSMPs localized at its surface. It is a magnetic-ordering crystal under the condition of low temperature [13] and its magnetic crystal cell contains two mutually staggered magnetic sublattices. Either magnetic sublattice is composed of atoms with the same magnetic moment, whereas the strong exchange field leads to that the atomic magnetic moments of the two sublattices are opposite in direction. It is more interesting that antiferromagnetically anisotropic field holds the atomic magnetic moments of the two sublattices to be parallel and antiparallel to the c axis (the easy axis), respectively. This AF is a uniaxial crystal without external magnetic field, whose permeability is negative in the plane normal to the easy axis and positive along the easy axis, and meanwhile its response frequency range is usually situated in the far infrared or THz-frequency region [14,15]. In the response frequency range, it supports ordinary surface magnon polaritons with the TE polarization and magnetostatic modes in the Voigt geometry [16–19]. As a new kind of naturally hyperbolic crystals, insulative AFs have been beginning to attract attention again [20–22]. In addition, we also noticed that another kind of surface magnon polariton was predicted at the interface between two identical enantiomeric antiferromagnets with the bianisotropy [23], where the uniaxial permittivity and permeability were used to determine dispersion properties of the surface magnon polaritons. These surface magnon polaritons were considered as a generalization of the Dyakonov surface waves.

[*]xzwang696@126.com
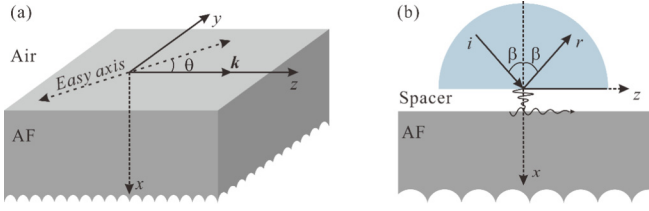
FIG. 1. Configurations and coordinate system used in the theoretical derivation and calculation, where the AF easy axis lies in the y-z plane or the AF surface and the space above the surface is filled with air. (a) For the derivation of dispersion equation, where θ is the propagating angle of DSMP with respect to the easy axis. (b) For the ATR calculation, where the AF and prism are separated by the air spacer, and β is the incident angle.

II. DISPERSION RELATIONS OF MAGNON POLARITONS

The AF permeability is a diagonal matrix in the principal-axis coordinate system (XYZ) [16,17,24] with the Z axis as the easy axis, whose diagonal elements are $\mu_0\mu_1$, $\mu_0\mu_1$, and μ_0, where μ_0 is the vacuum permeability. For an electromagnetic wave propagating along any direction, following Ref. [24], we find

$$\left(\frac{k_X^2 + k_Y^2}{n_e^2} + \frac{k_Z^2}{n_o^2} - \frac{\omega^2}{c^2}\right)\left(\frac{k^2}{n_o^2} - \frac{\omega^2}{c^2}\right) = 0, \quad (1)$$

where the indexes are determined by $n_e^2 = \varepsilon_a$ and $n_o^2 = \mu_1\varepsilon_a$ with relative dielectric constant ε_a, and ω and c are the angular frequency and vacuum light velocity. Equation (1) has two eigen wave solutions, whose dispersion equations are $k^2 = \mu_1\varepsilon_a f^2$ and $(k_X^2 + k_Y^2) + k_Z^2/\mu_1 = \varepsilon_a f^2$ with the reduced frequency $f = \omega/2\pi c$. In the case of $\mu_1 < 0$, the second dispersion equation exhibits a rotational hyperboloid of two sheets for a fixed frequency and corresponds to a propagating mode. It should be noted that the first dispersion equation does not represent any propagating mode in this case, but is related to an attenuated wave, or an evanescent wave. As a result, this AF is a hyperbolic material in this case. For our objective, the coordinate system and geometry that will be used are shown Fig. 1(a). We assume that a DSMP propagates along the z axis and its electromagnetic fields attenuate with the distance away from the surface. Therefore, the magnetic field of the DSMP is written as $\mathbf{H}' \exp(\Gamma' x + ikz - i\omega t)$ with $\Gamma' = (k^2 - \varepsilon' f^2)^{1/2}$ above the AF and $\mathbf{H} \exp(-\Gamma x + ikz - i\omega t)$ in the AF, where the vector in either magnetic-field expression is the field amplitude and meanwhile Γ' and Γ are the attenuation constants and positive real quantities. However, the AF permeability is a nondiagonal matrix in the xyz coordinate system with the z axis along the wave vector ($\mathbf{k}$) and is expressed with the following matrix (see the Appendix):

$$\overset{\leftrightarrow}{\mu} = \mu_0 \begin{pmatrix} 1+\chi & 0 & 0 \\ 0 & 1+\chi\cos^2\theta & \chi\sin\theta\cos\theta \\ 0 & \chi\sin\theta\cos\theta & 1+\chi\sin^2\theta \end{pmatrix}$$

$$= \mu_0 \begin{pmatrix} \mu_1 & 0 & 0 \\ 0 & \mu_{yy} & \mu_{yz} \\ 0 & \mu_{zy} & \mu_{zz} \end{pmatrix}. \quad (2)$$

$\chi = 2\omega_m\omega_a/(\omega_r^2 - \omega^2 - i\tau\omega)$ is the susceptibility and the characteristic frequencies and relevant physical parameters are connected with $\omega_m = 4\pi\gamma M_0$, $\omega_a = \gamma H_a$ and $\omega_r^2 = \gamma^2 H_a(2H_e + H_a)$, where H_a and H_e are the anisotropic and exchange fields, but M_0 is the sublattice magnetization, and meanwhile τ and γ are the damping constant and the gyromagnetic ratio [14,25]. In the AF, the field amplitude of DSMP satisfies the equations as follows:

$$-ik\Gamma H_z + [k^2 - \varepsilon_a\mu_1 f^2]H_x = 0, \quad (3a)$$

$$(k^2 - \Gamma^2 - \varepsilon_a\mu_{yy}f^2)H_y - \varepsilon_a\mu_{yz}f^2H_z = 0, \quad (3b)$$

$$-ik\Gamma H_x + (-\Gamma^2 - \varepsilon_a\mu_{zz}f^2)H_z - \varepsilon_a\mu_{yz}f^2H_y = 0. \quad (3c)$$

It is obvious that the coefficient determinant must be zero in Eqs. (3) for nonzero solutions of $\mathbf{H}$. Thus, we find that there are two evanescent-wave solutions (or two wave branches) in the AF, which correspond to

$$\Gamma_\pm^2 = [-b \pm (b^2 - 4\mu_1 c)^{1/2}]/2\mu_1, \quad (4)$$

with

$$b = -\mu_{zz}(k^2 - \varepsilon_a\mu_1 f^2) - \mu_1(k^2 - \varepsilon_a\mu_{yy}f^2), \quad (5a)$$

$$c = (k^2 - \varepsilon_a\mu_1 f^2)[\mu_{zz}(k^2 - \varepsilon_a\mu_{yy}f^2) + \varepsilon_a\mu_{yz}^2 f^2]. \quad (5b)$$

For convenience of discussion, we ignored the damping term included in χ, so both $\Gamma_\pm$ should be positive real quantities for a DSMP. We recognize that Eq. (4) should be reduced into more concise expressions. It has been noticed that

$$A = b^2 - 4\mu_1 c = [\mu_1(k^2 - \mu_{yy}\varepsilon_a f^2) - \mu_{zz}(k^2 - \mu_1\varepsilon_a f^2)]^2$$
$$- 4\mu_1\varepsilon_a(\mu_{yz}f)^2(k^2 - \mu_1\varepsilon_a f^2), \quad (6)$$

and substituting $\mu_1 - \mu_{zz} = \chi\cos^2\theta$ and $\mu_{zz} - \mu_{yy} = \chi(\sin^2\theta - \cos^2\theta)$ into (6) leads to

$$A = [\chi(k\cos\theta)^2 + \mu_1\chi\varepsilon_a f^2(\sin^2\theta - \cos^2\theta)]^2$$
$$- 4\mu_1\varepsilon_a(f\chi\sin\theta\cos\theta)^2(k^2 - \mu_1\varepsilon_a f^2). \quad (7)$$

Further to simplify this expression, we achieve

$$A = \chi^2[(k\cos\theta)^2 - \mu_1\varepsilon_a f^2]^2. \quad (8)$$

After substituting (8) into (4), the two attenuation constants are reduced into

$$\Gamma_+ = (\mu_{zz}k^2/\mu_1 - \varepsilon_a f^2)^{1/2}, \quad (9a)$$

$$\Gamma_- = (k^2 - \mu_1\varepsilon_a f^2)^{1/2}. \quad (9b)$$

The magnetic field of a DSMP in the AF should be the sum of the two branch fields corresponding to Γ_+ and Γ_-, i.e., $[\mathbf{H}^+ \exp(-\Gamma_+ x) + \mathbf{H}^- \exp(-\Gamma_- x)] \exp(ikz - i\omega t)$. The three field components of either branch are coupled together in the AF response-frequency range, so we can express the other components as functions of the z component. According to Eqs. (3b) and (9b) as well as $\nabla \cdot (\boldsymbol{\mu} \cdot \boldsymbol{H}) = 0$, we find

$$H_y^- = cgt\theta H_z^- = \lambda_- H_z^-, \quad H_x^- = \frac{ik}{\mu_1\Gamma_-}(\mu_{zz} + \mu_{yz}cgt\theta)H_z^-$$

$$= ikH_z^-/\Gamma_- \quad (10)$$

for the Γ_- branch. Also applying Eqs. (3b) and (9b), and noticing $\mu_1 - \mu_{yy} = \chi \sin^2\theta$, we achieve

$$H_y^+ = \frac{\varepsilon_a f^2 \chi \sin\theta \cos\theta}{\Gamma_-^2 - \Gamma_+^2 + \varepsilon_a \chi f^2 \sin^2\theta} H_z^+ = \lambda_+ H_z^+,$$

$$H_x^+ = \frac{ik}{\mu_1 \Gamma_+}(1 + \chi \sin^2\theta + \chi \sin\theta \cos\theta \lambda_+)H_z^+ \quad (11)$$

for the Γ_+ branch. Solving the dispersion equation of DSMP must involve the electromagnetic boundary conditions, so relations between the magnetic fields and relevant electric fields in the different spaces will be used. Due to $\mathbf{E} = \nabla \times \mathbf{H}/(-i\varepsilon_0\varepsilon\omega)$, and Eqs. (3a) and (9), it is obvious that

$$E_x^\pm = \frac{k}{\varepsilon_0\varepsilon_a\omega}H_y^\pm, \quad E_y^\pm = \frac{\mu_1 f^2 \Gamma_\pm}{i\varepsilon_0\omega\Gamma_-^2}H_z^\pm, \quad E_z^\pm = \frac{\Gamma_\pm}{i\varepsilon_0\varepsilon_a\omega}H_y^\pm \quad (12a)$$

in the AF. However,

$$E_x' = \frac{k}{\varepsilon_0\varepsilon'\omega}H_y', \quad E_y' = \frac{f^2}{-i\varepsilon_0\omega\Gamma'}H_z', \quad E_z' = \frac{\Gamma'}{-i\varepsilon_0\varepsilon'\omega}H_y' \quad (12b)$$

with $\Gamma' = (k^2 - \varepsilon' f^2)^{1/2}$ above the AF. Applying the four boundary-condition equations ($H_y' = H_y^+ + H_y^-$, $H_z' = H_z^+ + H_z^-$, $E_y' = E_y^+ + E_y^-$, and $E_z' = E_z^+ + E_z^-$) at the surface, the two equations are found to be

$$(\varepsilon_a\Gamma' + \varepsilon'\Gamma_-)\lambda_-H_z^- + (\varepsilon_a\Gamma' + \varepsilon'\Gamma_+)\lambda_+H_z^+ = 0, \quad (13a)$$

$$(1 + \Delta\Gamma_-)H_z^- + (1 + \Delta\Gamma_+)H_z^+ = 0, \quad (13b)$$

where $\Delta = \mu_1\Gamma'/\Gamma_-^2$. The determinant of coefficient matrix in Eqs. (13) must be equal to 0 for the existence of wave solution, i.e.,

$$(1 + \Delta\Gamma_+)(\varepsilon_a\Gamma' + \varepsilon'\Gamma_-)\lambda_- - (1 + \Delta\Gamma_-)(\varepsilon_a\Gamma' + \varepsilon'\Gamma_+)\lambda_+$$
$$= 0. \quad (14)$$

In order to obtain a concise and explicit dispersion relation like that found by Dyakonov [1], substituting the expressions of $\lambda_\pm$ and Δ into Eq. (14) and then simplifying this equation, we achieve

$$(\varepsilon_a\Gamma' + \varepsilon'\Gamma_-)(\Gamma_-^2 - \Gamma_+^2)(\mu_1\Gamma'\Gamma_+ + \Gamma_-^2) + \varepsilon_a\chi(f\sin\theta)^2$$

$$[\varepsilon'\Gamma_-^2(\Gamma_- - \Gamma_+) + \varepsilon_a\mu_1\Gamma'^2(\Gamma_+ - \Gamma_-)] = 0. \quad (15)$$

Finally, an explicit dispersion relation is found to be

$$(\varepsilon_a\Gamma' + \varepsilon'\Gamma_-)(\Gamma_- + \Gamma_+)(\mu_1\Gamma'\Gamma_+ + \Gamma_-^2)$$

$$+ \varepsilon_a(\mu_1 - 1)(\varepsilon' - \varepsilon_a\mu_1)(kf\sin\theta)^2 = 0. \quad (16)$$

It should be noted that either branch in the AF generally is neither a TE wave nor a TM wave, which is unlike the usual surface magnon polaritons.

Subsequently, we are going to discuss the dispersion equation. We first focus on some extreme cases. (1) In the case of $\theta \to 90°$ (in the Voigt geometry), due to $\varepsilon_a f^2(\mu_1 - 1) = (\Gamma_+^2 - \Gamma_-^2)$ and $k^2(\varepsilon' - \mu_1\varepsilon_a) = (\Gamma_-^2 - \mu_1\varepsilon_a\Gamma'^2)$ with $\Gamma_+ = \sqrt{k^2 - \varepsilon_a f^2}$ and $\Gamma_- = \sqrt{k^2 - \varepsilon_a\mu_1 f^2}$, Eq. (16) is

simplified into

$$\mu_1\Gamma' + \Gamma_- = 0, \quad (17)$$

which represents an ordinary surface magnon polariton with the TE polarization [14,17,18,25,26]. It is proven that this surface magnon polariton with an additional condition ($\Gamma_+ > 0$) is an extreme example of DSMP. (2) In the case of $\theta \to 0°$ (in the Faraday geometry), Eq. (16) degenerates into

$$\mu_1\Gamma'\Gamma_+ + \Gamma_-^2 = 0, \quad (18)$$

with $\Gamma_+ = (\mu_1^{-1}k^2 - \varepsilon_a f^2)^{1/2}$ and $\Gamma_- = (k^2 - \varepsilon_a\mu_1 f^2)^{1/2}$ that are positive real quantities. We recognize that Eq. (18) cannot be satisfied in this case since either Γ_+ is imaginary for $\mu_1 < 0$ or Eq. (18) is invalid for $\mu_1 > 0$. As a result, no DSMP exists in this case. (3) In the case of $k \to \infty$ (or $f \to 0$, the magnetostatic limit [14,17]), $\Gamma_- \to \Gamma' \to k$ and $\Gamma_+ \to k(\mu_{zz}\mu_1^{-1})^{1/2}$, so Eq. (16) becomes

$$1 + \mu_{zz} + (1 + \mu_1)\sqrt{\frac{\mu_{zz}}{\mu_1}} = 0. \quad (19)$$

It is obvious that there can be a solution for $\mu_{zz}/\mu_1 > 0$ and this solution is situated in the range of $\mu_1 < -1$. This solution should be called a Dyakonov surface magnon or Dyakonov surface spin wave. Its attenuation constant above the AF is equal to k and the two constants in the AF are k and $k(\mu_{zz}/\mu_1)^{1/2}$ that decreases as the propagating angle is decreased for a fixed value of k. Its magnetic-field amplitude has three components: $H_x' = -iH_z'$, H_y' and H_z' above the AF. $H_x^- = iH_z^-$ and $H_x^+ = i(\mu_{zz}/\mu_1)^{1/2}H_z^+$, $H_y^- = ctg\theta H_z^-$ and $H_y^+ = 0$, and H_z^- and H_z^+ in the AF. The magnetic-field amplitude indicates the polarization of DSM.

In normal circumstances, Eq. (16) implies the two possibilities for the existence of DSMP. The first possibility is that the first term is negative and the second term is positive on the left side of Eq. (16), but the most elementary condition $\mu_1 < 0$ must be satisfied. However, the second term cannot be positive under this condition, so this possibility should be ruled out. The second possibility is that the first term is positive and the second term is negative. It demands $(\mu_1 - 1)(\varepsilon' - \varepsilon_a\mu_1) < 0$. This demand corresponds to two conditions. The first condition is

$$\mu_1 < 1, \text{ or } \mu_1 < \varepsilon'\varepsilon_a^{-1}, \quad (20)$$

and the second condition is

$$\mu_1 > 1, \text{ or } \mu_1 > \varepsilon'\varepsilon_a^{-1}. \quad (21)$$

$\varepsilon_a > 1$ for an insulative AF and $\varepsilon' = 1$ if the space above the surface is filled with air, so $\mu_1 < \varepsilon_a^{-1}$ and $\mu_1 > 1$ are more valuable to be discussed in practice. The subsequently numerical calculation will show that no DSMP exists in the case of $\mu_1 > 1$. Therefore, $\mu_1 < \varepsilon'\varepsilon_a^{-1}$ or $\mu_1 < \varepsilon_a^{-1}$ is the necessary condition for the existence of DSMPs. It will be proven in the subsequent numerical results.

III. DERIVATION OF ATTENUATED TOTAL REFLECTION

The attenuated total reflection (ATR) method is very usable for physicists to observe surface polaritons in experiment [17,18]. Following this method with the configuration shown in Fig. 1(b), we can numerically calculate ATR spectra to

further examine the existence of the surface polaritons since a complicated dispersion equation may bring about nonphysical solutions. If a radiation incident on the bottom surface of the prism is totally reflected, a relevant evanescent wave is produced in the spacer below the bottom surface. This evanescent wave can excite DSMPs in the AF, as illustrated Fig. 1(b). The excitation of DSMPs absorbs the energy of incident radiation, so the reflective ratio is obviously decreased. We are going to derive the reflective ratio according to the electromagnetic boundary conditions. The electric fields in various spaces are

written as follows:

$$
\mathbf{E} = e^{ikz-i\omega t}
\begin{cases}
\mathbf{E}^i e^{ik_x x} + \mathbf{E}^r e^{-ik_x x}, & \text{(in the prism)} \\
\mathbf{A} e^{\Gamma' x} + \mathbf{B} e^{-\Gamma' x}, & \text{(in the spacer)} \\
\mathbf{E}^- e^{-\Gamma_- x} + \mathbf{E}^+ e^{-\Gamma_+ x}, & \text{(in the AF)}
\end{cases}
\quad (22)
$$

where superscripts i and r indicate incidence and reflection, and meanwhile $k_x = f\sqrt{\varepsilon_p}\cos\beta$ and $k = f\sqrt{\varepsilon_p}\sin\beta$ with dielectric constant ε_p of the prism and incident angle β. The relevant magnetic fields can be determined with $\overset{\leftrightarrow}{\mu} \cdot \mathbf{H} = \nabla \times \mathbf{E}/i\omega$. In the prism and spacer,

$$
H_z = e^{ikz-i\omega t}
\begin{cases}
k_x \left(E_y^i e^{ik_x x} - E_y^r e^{-ik_x x} \right)/\mu_0 \omega, & \text{(in the prism)} \\
\Gamma'(A_y e^{\Gamma' x} - B_y e^{-\Gamma' x})/i\mu_0 \omega, & \text{(in the spacer)}
\end{cases},
\quad (23a)
$$

$$
H_y = e^{ikz-i\omega t}
\begin{cases}
-i\varepsilon_p f^2 \left(E_z^i e^{ik_x x} - E_z^r e^{-ik_x x} \right)/i\mu_0 \omega k_x, & \text{(in the prism)} \\
f^2(A_z e^{\Gamma' x} - B_z e^{-\Gamma' x})/i\mu_0 \omega \Gamma', & \text{(in the spacer)}
\end{cases}.
\quad (23b)
$$

In the AF,

$$
H_z = e^{ikz-i\omega t} \sum_{j=-}^{j=+} \frac{\mu_{yz}(k^2 - \Gamma_j^2)E_z^j - \mu_{yy}\Gamma_j^2 E_y^j}{i\mu_0 \mu_v^y \mu_{yy}\omega \Gamma_j} e^{-\Gamma_j x}
$$

$$
= H_z^- + H_z^+, \quad (24a)
$$

$$
H_y = e^{ikz-i\omega t} \sum_{j=-}^{j=+} \frac{\mu_{zz}(\Gamma_j^2 - k^2)E_z^j + \mu_{yz}\Gamma_j^2 E_y^j}{i\mu_0 \mu_v^z \mu_{zz}\omega \Gamma_j} e^{-\Gamma_j x}
$$

$$
= H_y^- + H_y^+, \quad (24b)
$$

where $\mu_v^y = (\mu_{yy}\mu_{zz} - \mu_{yz}^2)/\mu_{yy}$ and $\mu_v^z = (\mu_{yy}\mu_{zz} - \mu_{yz}^2)/\mu_{zz}$. In addition, $H_y^\pm = \lambda_\pm H_z^\pm$ with $\lambda_\pm$ defined by Eqs. (10) and (11) in the above section. According to Eqs. (24), the relation between the two electric-field components in the AF is achieved to be

$$
E_y^\pm = \frac{(k^2 - \Gamma_\pm^2)(\mu_{zz} + \mu_{yz}\lambda_\pm)}{\Gamma_\pm^2(\mu_{yz} + \mu_{yy}\lambda_\pm)}E_z^\pm = \Lambda_\pm E_z^\pm.
\quad (25)
$$

The electromagnetic boundary conditions at the two surfaces of the spacer, the continuity of E_y and H_z, lead to the following equations:

$$
\begin{pmatrix} A_y \\ B_y \end{pmatrix} = \frac{1}{2}\begin{pmatrix} \gamma_+ & \gamma_- \\ \gamma_- & \gamma_+ \end{pmatrix}\begin{pmatrix} E_y^i \\ E_y^r \end{pmatrix}, \quad \begin{pmatrix} A_y \\ B_y \end{pmatrix} = \frac{1}{2}\overset{\leftrightarrow}{T}\begin{pmatrix} E_z^- \\ E_z^+ \end{pmatrix},
\quad (26)
$$

with $\gamma_\pm = 1 \pm ik_x/\Gamma'$, in which elements of $\overset{\leftrightarrow}{T}$ are

$$
T_{11} = \left[\frac{\mu_{yz}(k^2 - \Gamma_-^2) - \mu_{yy}\Gamma_-^2 \Lambda_-}{\mu_v^y \mu_{yy}\Gamma' \Gamma_-} + \Lambda_- \right]e^{-\Gamma' d}, \quad (27a)
$$

$$
T_{12} = \left[\frac{\mu_{yz}(k^2 - \Gamma_+^2) - \mu_{yy}\Gamma_+^2 \Lambda_+}{\mu_v^y \mu_{yy}\Gamma' \Gamma_+} + \Lambda_+ \right]e^{-\Gamma' d}, \quad (27b)
$$

$$
T_{21} = \left[-\frac{\mu_{yz}(k^2 - \Gamma_-^2) - \mu_{yy}\Gamma_-^2 \Lambda_-}{\mu_v^y \mu_{yy}\Gamma' \Gamma_-} + \Lambda_- \right]e^{\Gamma' d}, \quad (27c)
$$

$$
T_{22} = \left[-\frac{\mu_{yz}(k^2 - \Gamma_+^2) - \mu_{yy}\Gamma_+^2 \Lambda_+}{\mu_v^y \mu_{yy}\Gamma' \Gamma_+} + \Lambda_+ \right]e^{\Gamma' d}. \quad (27d)
$$

Meanwhile, applying the continuity of E_z and H_y at the two surfaces of the spacer, we find the relations

$$
\begin{pmatrix} A_z \\ B_z \end{pmatrix} = \frac{1}{2}\begin{pmatrix} \gamma'_- & \gamma'_+ \\ \gamma'_+ & \gamma'_- \end{pmatrix}\begin{pmatrix} E_z^i \\ E_z^r \end{pmatrix}, \quad \begin{pmatrix} A_z \\ B_z \end{pmatrix} = \frac{1}{2}\overset{\leftrightarrow}{S}\begin{pmatrix} E_z^- \\ E_z^+ \end{pmatrix},
\quad (28)
$$

with $\gamma'_\pm = 1 \pm i\varepsilon_p \Gamma'/k_x$, where elements of $\overset{\leftrightarrow}{S}$ are shown with

$$
S_{11} = \left\{ \frac{\Gamma'[\mu_{zz}(\Gamma_-^2 - k^2) + \mu_{yz}\Gamma_-^2 \Lambda_-]}{f^2 \mu_v^z \mu_{zz}\Gamma_-} + 1 \right\}e^{-\Gamma' d}, \quad (29a)
$$

$$
S_{12} = \left\{ \frac{\Gamma'[\mu_{zz}(\Gamma_+^2 - k^2) + \mu_{yz}\Gamma_+^2 \Lambda_+]}{f^2 \mu_v^z \mu_{zz}\Gamma_+} + 1 \right\}e^{-\Gamma' d}, \quad (29b)
$$

$$
S_{21} = \left\{ \frac{\Gamma'[\mu_{zz}(k^2 - \Gamma_-^2) - \mu_{yz}\Gamma_-^2 \Lambda_-]}{f^2 \mu_v^z \mu_{zz}\Gamma_-} + 1 \right\}e^{\Gamma' d}, \quad (29c)
$$

$$
S_{22} = \left\{ \frac{\Gamma'[\mu_{zz}(k^2 - \Gamma_+^2) - \mu_{yz}\Gamma_+^2 \Lambda_+]}{f^2 \mu_v^z \mu_{zz}\Gamma_+} + 1 \right\}e^{\Gamma' d}. \quad (29d)
$$

Eliminating $A_{y,z}$, $B_{y,z}$, and $E_z^\pm$ in Eqs. (26) and (28), we obtain the equation satisfied by the amplitudes of reflective electric field, i.e.,

$$
\begin{pmatrix} E_y^i \\ E_y^r \end{pmatrix} = \overset{\leftrightarrow}{P}{}^{-1}\overset{\leftrightarrow}{T}\overset{\leftrightarrow}{S}{}^{-1}\overset{\leftrightarrow}{P}'\begin{pmatrix} E_z^i \\ E_z^r \end{pmatrix},
\quad (30)
$$

where P is the 2×2 matrix in the first equation of Eqs. (26) and P' is the 2×2 matrix in the first equation of Eqs. (28). It should be noted that the damping term in the permeability must be considered for calculating ATR spectra. Therefore, Γ' and $\Gamma_\pm$ are complex values at present.

IV. NUMERICAL RESULTS AND DISCUSSION

Numerical calculations are based on the FeF$_2$ crystal with dielectric constant $\varepsilon_a = 5.5$ and the gyromagnetic ratio $\gamma = 1.97$(rad/skG). The other physical parameters are the sublattice magnetization $4\pi M_0 = 7.04$ kG ($\omega_m = 0.736$ cm^{-1}), the exchange field $H_e = 540.0$ kG ($\omega_e = 56.44$ cm^{-1}), anisotropic field $H_a = 200.0$ kG ($\omega_a = 20.9$ cm^{-1}) [18,26,27]. The AF resonant frequency is $\omega_r = 52.877$ cm^{-1} and the zero-point frequency of μ_1 is
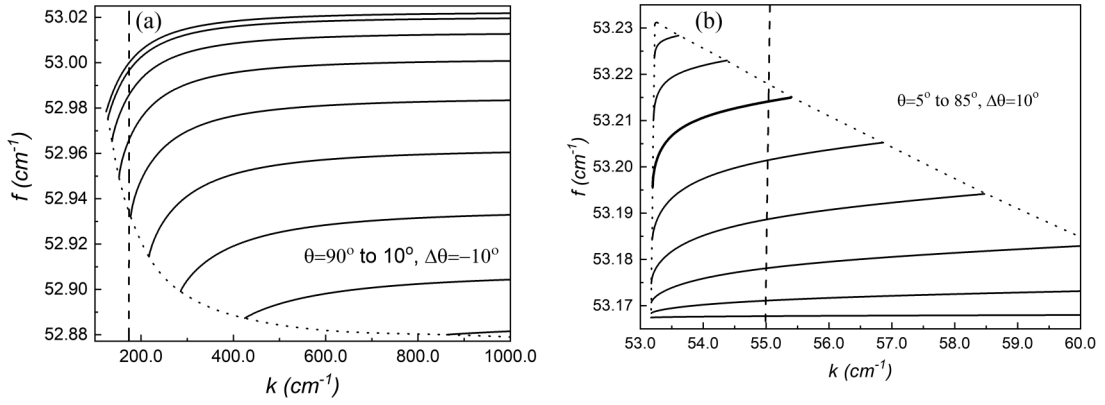
FIG. 2. Dispersion curves of DSMPs for various propagating angles, where $\Delta\theta$ is the propagating-angle difference between two adjacent curves and the vertical dashed lines represent the scanning lines for numerical calculating ATR. (a) Dispersion curves of the first DSMP, where the topmost curve is related to $\theta = 90°$ and the dotted curve is the left boundary of the area where the first DSMP exists. (b) Dispersion curves of the second DSMP, where the topmost curve corresponds to $\theta = 5°$ and the two dotted lines are the left and right boundaries of the region in which the second DSMP appears.

53.165 cm^{-1}. The AF is a magnetically hyperbolic material between the two special frequencies, otherwise it is an ellipse material. We propose that the space above the AF surface is filled with air, or $\varepsilon' = 1.0$. The damping constant is taken as $\tau = 0.01 \text{ cm}^{-1}$ for ATR numerical calculations.

From dispersion relation (16), we find two DSMPs, as shown in Fig. 2. Figure 2(a) and Fig. 3(a) show properties of the first DSMP as follows. It is situated inside the reststrahlen frequency band and is a large wave-vector mode. Any dispersion curve of this DSMP begins from the left endpoint corresponding to $\Gamma_+ = 0$ and infinitely extends rightward, and meanwhile its frequency increases with k. It is very interesting that the first DSMP possesses its magnetostatic limit. In this limit, this DSMP becomes DSM whose dispersion equation is Eq. (19). Figure 3(b) illustrates the dispersion curve of the DSM, i.e., its frequency versus its propagating angle. Com-

bining the discussion about Eq. (19) in the previous section, we conclude that the DSM and first DSMP occupies only a part of the reststrahlen frequency band and $\mu_1 < -1$ is the necessary condition for the existence of the DSM and first DSMP. They are situated in the light-gray region in Fig. 3(a). The DSM also can be considered as a Dyakonov-like surface spin wave. Figure 2(b) illustrates the second DSMP. It lies outside the reststrahlen frequency band and is localized in a special frequency range where $0 < \mu_1 < \varepsilon_a^{-1}$ and the AF is an ellipse material. This frequency range is the gray region in Fig. 3(a). Any dispersion curve of the second DSMP is finite. The left endpoint of the dispersion curve corresponds to $\Gamma' = 0$ and its right endpoint is related to $\Gamma_+ = 0$. Unlike the first DSMP, the second DSMP has no magnetostatic limit and its wave vector is much smaller than that of the first DSMP, and meanwhile it disappears in the Voigt geometry ($\theta = 90°$).

Subsequently, we discuss the localization of either DSMP at the AF surface, which is reflected by the attenuation constants. It should be noted that either DSMP involves three attenuation constants. One is Γ' in the space above the AF surface, and the other two are Γ_+ and Γ_- attached to the two wave branches in the AF. In normal circumstances, the two wave branches are attenuated in desynchrony with distance away from the AF surface. The larger either attenuation constant in the AF is, the higher the localization of the relevant branch is. Figure 4 illustrates the attenuation constants of the two DSMPs. For the first DSMP, Fig. 4(a) shows that curves of the two attenuation constants in the AF are distributed above and below the line of Γ', respectively. It is obvious that $\Gamma_- > \Gamma'$ and $\Gamma_+ < \Gamma'$. The difference between Γ_+ and Γ_- increases as θ is decreased. In general, the first DSMP is of higher localization. For the second DSMP, the curves of two attenuation constants in the AF cross at a definite point. The curves of Γ_- are distributed above the line of Γ' and the major part of any Γ_+- curve is situated above the line of Γ', as shown in Fig. 4(b). In general, the second DSMP decays much more slowly above than below the AF surface.

The polarization of a surface polariton is one of its important characteristics. For the DSMPs and DSM, we use their
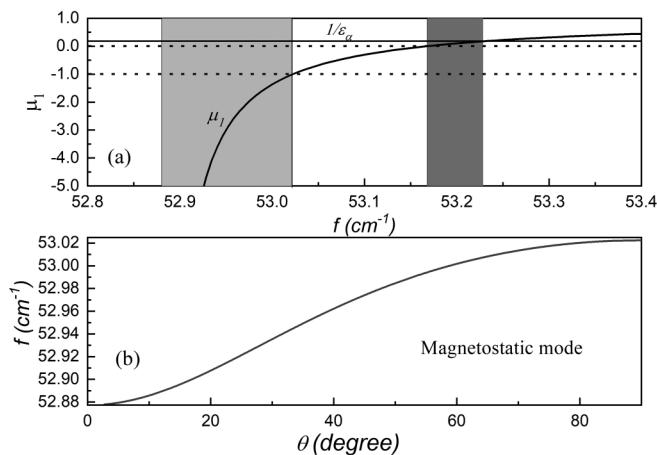
FIG. 3. (a) The permittivity and frequency regions occupied by DSMPs, where the first DSMP is situated in the light-gray region and the second DSMP lies in the gray region. The horizontal solid line corresponds to ε_a^{-1}, and the two horizontal dashed lines indicate the 0 line and -1 line. The solid curve shows the permittivity. (b) The dispersion curve of Dyakonov surface magnon; it occupies the light-gray region in (a).
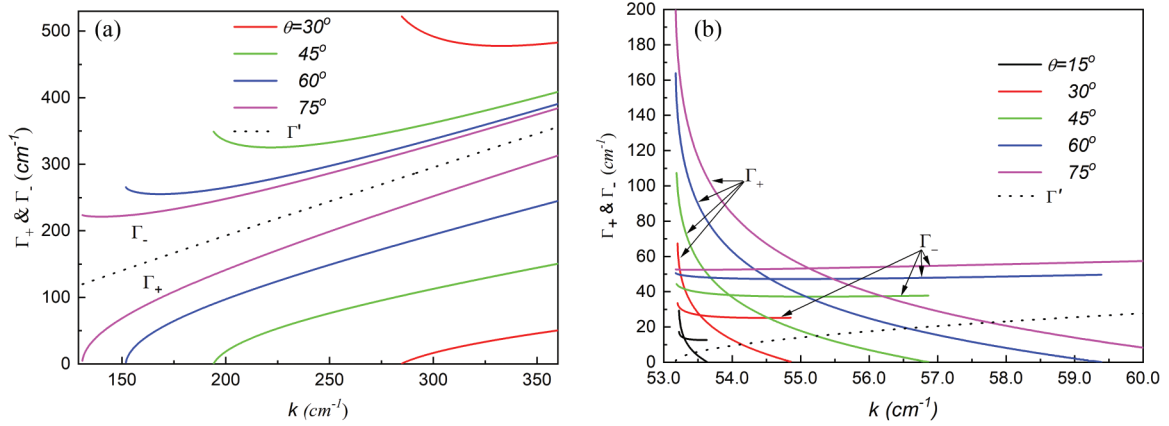
FIG. 4. Attenuation constants of DSMPs vs k for various propagating angles. (a) For the first DSMP and (b) for the second DSMP, where a pair of solid curves with the same color indicates Γ_+ and Γ_- in the AF, but the dotted line represents Γ' above the surface.

magnetic fields to uniformly discuss the features of polarization. The electromagnetic fields on and beneath the AF surface are coupled with together through the boundary conditions for any DSMP or DSM. We assume that the magnetic field on the AF surface is normalized with $|H'_x|^2 + |H'_x|^2 + |H'_z|^2 = 1$.

For the DSMPs, we can achieve magnetic-amplitude components on and beneath the surface. Due to Eqs. (10) and (11), we have

$$H'_y = \lambda_+ H_z^+ + \lambda_- H_z^-, \tag{31}$$

and further using Eq. (13b) and $H'_z = H_z^+ + H_z^-$, we obtain

$$H'_y = (\alpha\lambda_+ + \lambda_-)H_z^-, \; H'_z = (\alpha + 1)H_z^-, \tag{32}$$

with $\alpha = -(1 + \Delta\Gamma_-)/(1 + \Delta\Gamma_+)$. Thus, we find that

$$H'_y = (\alpha\lambda_+ + \lambda_-)H'_z/(1+\alpha), \; H'_x = -ikH'_z/\Gamma'. \tag{33}$$

It is obvious that H'_z can be written as

$$H'_z = \{1 + [(\lambda_- + \alpha\lambda_+)/(1+\alpha)]^2 + (k/\Gamma')^2\}^{-1/2}. \tag{34}$$

As a result, the magnetic-field amplitudes on and beneath the surface can be achieved from Eqs. (33) and (34).

For the DSM, simpler expressions of the magnetic-field amplitude can be obtained. In the magnetostatic limit, $\lambda_- = ctg\theta$, $\lambda_+ = 0$, $\Gamma_- = \Gamma' = k$, and $\Gamma_+ = k(\mu_{zz}\mu_1^{-1})^{1/2}$. In

addition, $\Delta = \mu_1/k$ and $\alpha = -(1+\mu_1)/(1+\Gamma_+)$. Therefore, we find the field-amplitude components on the surface to be

$$H'_z = \{2 + [ctg\theta/(1+\alpha)]^2\}^{-1/2}, \quad H'_y = ctg\theta H'_z/(1+\alpha),$$
$$H'_x = -iH'_z, \tag{35}$$

and those beneath the surface to be

$$H_z = H'_z, \quad H_y = H'_y, \quad H_x = i\left\{\frac{1}{1+\alpha} + \frac{\alpha}{1+\alpha}\sqrt{\frac{\mu_1}{\mu_{zz}}}\right\}H'_z. \tag{36}$$

Based on Sec. II and these formulas, we recognize that the x component of the magnetic-field amplitude is imaginary but the y- and z components are real for the DSMPs and DSM. It is proven that the phase difference between them is $\pi/2$. The magnetic field of the ordinary magnon [19] and magnon polariton [16–18] is in the x-z plane, but that of the DSMPs and DSM possesses three components.

We illustrate the polarization or magnetic-field amplitude of the DSMPs at the AF surface in Figs. 5 and 6. The boundary conditions mean that the parallel components of the magnetic field are continual at the surface, but the vertical component
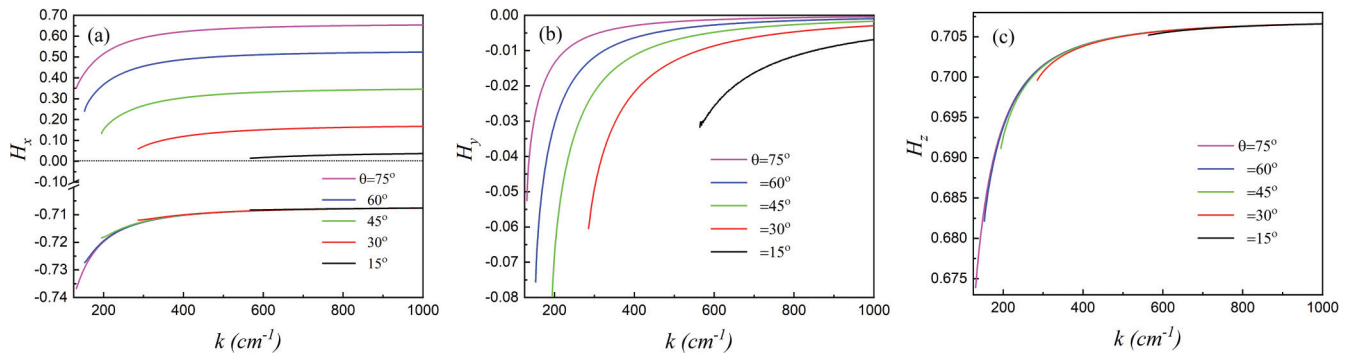
FIG. 5. The magnetic-field amplitude of the first DSMP vs k for various propagating angles. Its x components above and below the surface are imaginary and are different, and further the imaginary part is negative below the surface and positive above the surface. The y- or z components above and below the surface are real and the same.
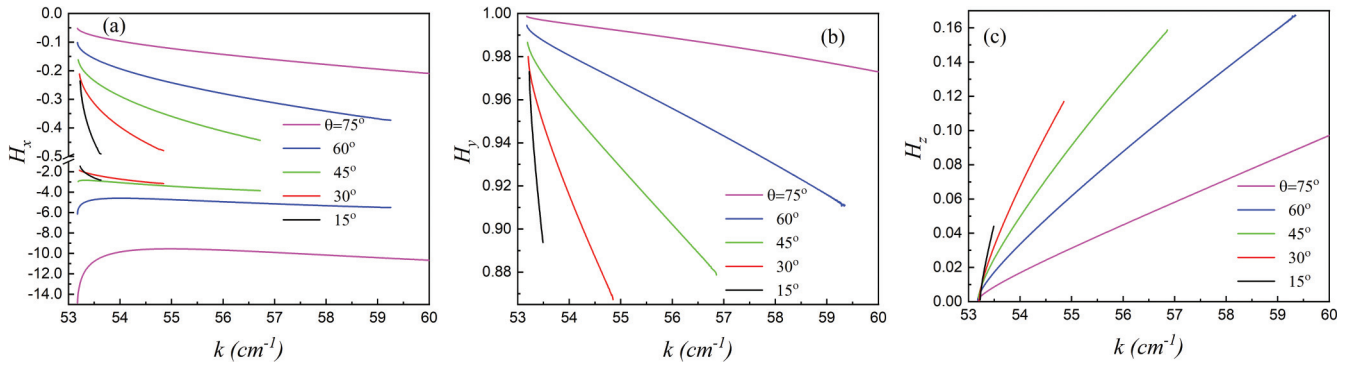
FIG. 6. The magnetic-field amplitude of the second DSMP vs k for various propagating angles. The x components above and below the surface are imaginary and different, and further the imaginary parts below and above the surface both are negative. The curves below the break indicate the amplitude in the AF. The y- or z components above and below the surface are real and the same.

on the surface is different from that beneath the surface. It should be noted that the x component is the vertical component and is imaginary, so its curves show its imaginary part in figures.

We first discuss the magnetic-field amplitude of the first DSMP, as illustrated in Fig. 5. Figure 5(a) indicates the x component without the real part. It is negative and approximately equal to -0.7 above the surface; its curves partly overlap for different propagating angles. However, it is positive below the surface and evidently changes with the propagating angle. Figure 5(b) shows that the y component is a small negative real quantity. Figure 5(c) indicates that the z component is a positive real quantity and comparable to the imaginary part of the x component in amplitude. It is obvious that the magnetic field is approximately situated in the x-z plane. Therefore, this polariton is a close approximation to a TE wave, especially for a larger propagating angle. We subsequently discuss the magnetic amplitude of the second DSMP, as illustrated in Fig. 6. Comparing the z component with the x- and y components, one finds that the field amplitude above the surface approximately lies in the x-y plane, but the field amplitude below the surface is approximately not only in the x-y plane but also further approximately along the x axis. In addition,

the x component of magnetic field is very intense in the AF, especially for large propagating angles.

We have found the two DSMPs from the dispersion equation. The first DSMP possesses the magnetostatic limit. However, it is necessary to further examine the existence of them since the complicated dispersion equation may include nonphysical solutions. The attenuated total reflection calculation is a numerical stimulation of relevant experiment and the results are believable for one to examine surface polaritons. The schematic diagram is shown in Fig. 1(b). In order to demonstrate the existence of the first DSMP with larger wave vector, we use the Si prism and a large incident angle $\beta = 75°$. The critical angle is $\beta_c = 19°$ for the total reflection from the bottom surface of the Si prism. According to the polarization features of the first DSMP, we use the TE incident radiation. For the second DSMP with smaller wave vector, we use the SiO$_2$ prism so that the critical angle $\beta_c = 41.1°$ and meanwhile we take the incident angle to be $\beta = 43°$. For this DSMP, we apply the TM incident radiation. At the two selected incident angles, the total reflection condition is satisfied, but the partial energy of incident radiation is absorbed to excite magnon polaritons in the AF, so the reflective ratio is decreased. The bulk polaritons occupy some continua in the
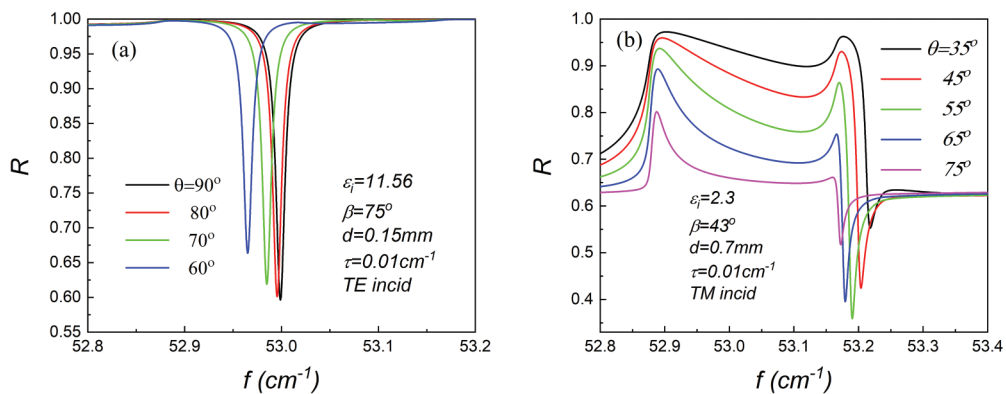
FIG. 7. The attenuated total reflective ratio vs frequency for various propagating angles. (a) is obtained from the transversely electric incidence. The four sharp dips show the first DSMP for the four propagating angles and correspond to the four intersections of the dispersion curves and the scanning line in Fig. 2(a), respectively. (b) comes from the transversely magnetic incidence. The five sharp dips demonstrate the second DSMP for the five propagating angles and correspond to the five intersections between the dispersion curves and the scanning line in Fig. 2(b), respectively.

f-k space, but surface polaritons are isolated curves, so the surface polaritons correspond to sharp dips on the ATR curves. A sharp dip on an ATR curve corresponds to a fixed frequency f and a definite wave vector k due to $k = f\sqrt{\varepsilon'}\sin\beta$. The dip represents the relevant surface polariton if the point (k, f) is just on the relevant dispersion curve. Figure 7(a) displays four sharp dips for four propagating angles, respectively. We recognize that the f and k values of each dip are just situated on the intersections of the dispersion curves and the scanning line in Fig. 2(a). It proves the real existence of the first DSMP. However, the ATR method cannot be used to examine surface polaritons with very large wave number, including magnetostatic modes or magnons. In this case, a light-scattering technique should be applied. Figure 7(b) exhibits five sharp dips for five propagating angles, respectively. We also find that the f and k values of every dip just lie on the intersection of the corresponding dispersion curve and scanning line in Fig. 2(b). Therefore, we also prove the existence of the second DSMP. In addition, the ATR spectra demonstrate the observability of DSMPs.

V. SUMMARY

We predicted one Dyakonov surface magnon and two Dyakonov magnon-polaritons supported by an antiferromagnet-air interface. The DSM is the magnetostatic limit of the first DSMP, which are situated in the reststrahlen frequency band of the antiferromagnet, more specifically in the frequency range of $\mu_1 < -1$. The first DSMP possesses large attenuation constants and a large wave vector so that it is highly localized at the AF surface. Due to the very small y component of its magnetic field, it is more similar to a TE surface wave. The second DSMP lies outside the reststrahlen band of the antiferromagnet and is specifically localized in the frequency region of $\varepsilon'\varepsilon_a^{-1} > \mu_1 > 0$. It has no magnetostatic limit, unlike the first DSMP. In polarization, the second DSMP is similar to neither a TE wave nor a TM wave. Compared with the first DSMP, its attenuation constants are relatively small. Both the DSMPs are hybrid-polarization surface waves, composed of the two branches with different polarizations in the AF. For the DSM, we have obtained the simple analytic expressions of its magnetic field and its attenuation constants. The DSM is a new magnon, i.e., a magnetostatic mode of hybrid polarization. We used the ATR spectra numerically calculated to examine the DSMPs obtained from the dispersion equation. According to their polarization features, the first DSMP was examined by the ATR spectra with TE incident radiation and the second DSMP was demonstrated by the ATR spectra with TM incident radiation. The results have proved the real existence of the two DSMPs and the observability in experiment. The

DSM should be measured by means of a light-scattering technique, and will be discussed in next work.

APPENDIX

In the XYZ coordinate system with the Z axis as the AF easy axis, the AF permeability without the external magnetic field is a diagonal sector, and

$$\mathbf{B}' = \overleftrightarrow{\mu}' \cdot \mathbf{H}', \tag{A1}$$

where $\mathbf{B}'$ is the magnetic induction and $\mathbf{H}'$ is the magnetic field. According to the geometry in Fig. 1(a), we should transfer Eq. (A1) into the expression in the xyz coordinate system or

$$\mathbf{B} = \overleftrightarrow{\mu} \cdot \mathbf{H}. \tag{A2}$$

Therefore, the expression of $\overleftrightarrow{\mu}$ in the xyz coordinate frame is achieved with a rotation transferring of the diagonal sector to be

$$\overleftrightarrow{\mu} = \mu_0 \begin{pmatrix} 1 & 0 & 0 \\ 0 & \cos\theta & -\sin\theta \\ 0 & \sin\theta & \cos\theta \end{pmatrix} \begin{pmatrix} \mu_1 & 0 & 0 \\ 0 & \mu_1 & 0 \\ 0 & 0 & 1 \end{pmatrix}$$
$$\times \begin{pmatrix} 1 & 0 & 0 \\ 0 & \cos\theta & \sin\theta \\ 0 & -\sin\theta & \cos\theta \end{pmatrix}, \tag{A3}$$

and further we find

$$\overleftrightarrow{\mu} = \mu_0 \begin{pmatrix} \mu_1 & 0 & 0 \\ 0 & \mu_1\cos^2\theta + \sin^2\theta & (\mu_1 - 1)\sin\theta\cos\theta \\ 0 & (\mu_1 - 1)\sin\theta\cos\theta & \mu_1\sin^2\theta + \cos^2\theta \end{pmatrix}, \tag{A4}$$

so the nonzero elements of the permeability sector in the xyz coordinate system are

$$\mu_{xx} = \mu_1, \quad \mu_{yy} = 1 + \chi\cos^2\theta, \quad \mu_{zz} = 1 + \chi\sin^2\theta, \tag{A5}$$

$$\mu_{yz} = \mu_{zy} = \chi\sin\theta\cos\theta, \tag{A6}$$

where $\mu_1 = 1 + \chi$ and χ is the AF susceptibility defined in the text.

[1] M. I. Dyakonov, New type of electromagnetic wave propagating at an interface, Sov. Phys. JETP **67**, 714 (1988).

[2] O. Takayama, L. Crasovan, D. Artigas, and L. Torner, Observation of Dyakonov Surface Waves, Phys. Rev. Lett. **102**, 043903 (2009).

[3] E. E. Narimanov, Dyakonov waves in biaxial anisotropic crystals, Phys. Rev. A **98**, 013818 (2018).

[4] D. Artigas and L. Torner, Dyakonov Surface Waves in Photonic Metamaerials, Phys. Rev. Lett. **94**, 013901 (2005).

[5] Q. Zhang, S. Zhou, S. F. Fu, and X. Z. Wang, Diversiform hybrid-polarization surface plasmon polaritons in a dielectric–metal metamaterial, AIP Adv. **7**, 045216 (2017).

[6] Q. Zhang, S. Zhou, S. F. Fu, and X. Z. Wang, Rich hybridized-polarization surface phonon polaritons in hyperbolic metamaterials, AIP Adv. **7**, 105211 (2017).

[7] J. A. Sorni, M. Naserpour, C. J. Zapata-Rodríguez, and J. J. Miret, Dyakonov surface waves in lossy metamaterials, Opt. Commun. **355**, 252 (2015).

[8] I. V. Fedorin, Surface polaritons and Dyakonov-like surface waves in an isotropic-anisotropic nanocomposite system, J. Phys: Conf. Series **1092**, 012033 (2018).

[9] Y. Zhang, X. Wang, D. Zhang, S. Fu, S. Zhou, and X.-Z. Wang, Unusual spin and angular momentum of Dyakonov waves at hyperbolic-material surface, Opt. Express **28**, 19205 (2020).

[10] S. Fu, S. Zhou, Q. Zhang, and X.-Z. Wang, Completely confinement and extraordinary propagation of Dyakonov-like polaritons in hBN, Opt. Laser Technol. **125**, 106012 (2019).

[11] C. J. Zapata-Rodríguez, J. J. Miret, S. Vuković, and M. R. Belić, Engineered surface waves in hyperbolic metamaterials, Opt. Express **21**, 19113 (2013).

[12] E. Cojocaru, Comparative analysis of Dyakonov hybrid surface waves at dielectric–elliptic and dielectric–hyperbolic media interfaces, J. Opt. Soc. Am. B **31**, 2558 (2014).

[13] S. V. Vonsovskii, *Magnetism* (Keter Publishing House Jerusalem Ltd, Jerusalem, 1974), Vol. 2, Chap. 22.

[14] K. Abraha and D. R. Tilley, Theory of far infrared properties of magnetic surfaces, films and superlattices, Surf. Sci. Rep. **24**, 129 (1996).

[15] R. L. Stamps and R. E. Camley, Green's function for antiferromagnetic polaritons, I. Surface modes and resonances, Phys. Rev. B **40**, 596 (1996).

[16] R. E. Camley and D. L. Mills, Surface-polaritons on uniaxial antiferromagnets, Phys. Rev. B **26**, 1280 (1982).

[17] M. G. Cottam and D. R. Tilley, *Introduction to Surface and Superlattice Excitations* (IOP Publishing Ltd, Philadelphia, 2005), Chaps. 6 and 9.

[18] M. R. F. Jensen, T. J. Parker, K. Abraha, and D. R. Tilley, Experimental Observation of Surface Magnetic Polaritons in FeF_2 by Attenuated Total Reflection (ATR), Phys. Rev. Lett. **75**, 3756 (1995).

[19] B. Luthi, D. L. Mills, and R. E. Camley, Surface spin waves in antiferromagnets, Phys. Rev. B **28**, 1475 (1983).

[20] R. Macêdo and R. E. Camley, Engineering terahertz surface magnon-polaritons in hyperbolic antiferromagnets, Phys. Rev. B **99**, 014437 (2019).

[21] V. B. Silva and T. Dumelow, Surface mode enhancement of the Goos-Hänchen shift in direct reflection off antiferromagnets, Phys. Rev. B **97**, 235158 (2018).

[22] K. Grishunin, T. Huisman, G. Li, E. Mishina, T. Rasing, A. V. Kimel, K. Zhang, Z. Jin, S. Cao, W. Ren, G.-H. Ma, and R. V. Mikhaylovskiy, Terahertz magnon-polaritons in $TmFeO_3$, ACS Photonics **5**, 1375 (2018).

[23] R. H. Tarkhanyan, New class of surface magnon polaritons in enantiomeric antiferromagnetic structures, Prog. Electromagn. Res. B **39**, 55 (2012).

[24] A. Yariv and P. Yeh, *Optical Waves in Crystals* (John Wiley & Sons Inc., New York, 1984), Chap. 4.

[25] X.-Z. Wang and D. R. Tilley, Retarded modes of a lateral antiferromagnetic/nonmagnetic superlattice, Phys. Rev. B **52**, 13353 (1995).

[26] C. Jia, X.-Z. Wang, and S.-C. Lu, Effects of eddy currents on retarded modes of antiferromagnet, Phys. Rev. B **59**, 3310 (1999).

[27] X.-Z. Wang and H. Li, Nonlinear polaritons in antiferromagnetic/nonmagnetic superlattices, Phys. Rev. B **72**, 054403 (2005).